



Relationship between microstructure and mechanical properties of 5083 aluminum alloy thick plate

Xin-wei SHE^{1,2}, Xian-quan JIANG^{1,2}, Pu-quan WANG¹, Bin-bin TANG¹, Kang CHEN¹, Yu-jie LIU¹, Wei-nan CAO¹

1. School of Materials and Energy, Southwest University, Chongqing 400715, China;

2. Advanced Materials Research Center, Chongqing Academy of Science and Technology, Chongqing 401123, China

Received 18 October 2019; accepted 16 June 2020

Abstract: The microstructure and mechanical properties of 105 mm thick 5083 aluminum alloy hot rolled plate were investigated by metallurgical microscope, scanning electron microscope and tensile testing machine, and three major characteristic problems in mechanical properties inhomogeneity were explained. The results show that the mechanical properties of the rolled plate are inhomogeneous along the thickness direction. From the surface to the center, the strength shows an inverted “N” shape change and the elongation presents a semi “U” shape change. Several similar structural units composed of long fibrous grains (LFG) and short fibrous grains bands (SFGB) exist in a special layer (Layer 2) adjacent to the surface. This alternating layered distribution of LFG and SFGB is conducive to improving the plasticity by dispersing the plastic deformation concentrated on the boundary line (BL) between them. However, their different deformability will cause the alternation of additional stresses during the hot rolling, leading to the strength reduction. The closer the location to the center of the plate is, the more likely the recovery rather than the recrystallization occurs. This is the possible reason for the unnegligible difference in strength near the central region (Layer 4 and Layer 5).

Key words: aluminum alloy thick plate; mechanical properties; inhomogeneity; fibrous grains; dynamic recovery; dynamic recrystallization

1 Introduction

Aluminum alloys are widely used in aerospace, transportation and national defense industry due to their light mass, great corrosion resistance, high strength, excellent processing performance and low cost [1–3]. In recent years, a large number of researchers have focused on the relationship among microstructure, hot deformation, heat treatment and mechanical properties of aluminum alloy thin plates, while there have been few reports about the inhomogeneity of microstructure and mechanical properties of thick plates [4–8].

It is known that the inhomogeneity of

microstructure and mechanical properties of aluminum alloy thick plates along the thickness direction is related to the alloy composition, second phase distribution and texture type, and it will become more obvious with the increase of the plate thickness. CHANG et al [9] carried out an intensive research on the structure and texture of 20 mm thick 7056 aluminum alloy, and found that the recrystallization degree increased gradually from the surface to the center, the volume fraction of recrystallization textures (Cube {001}<100>) in the surface was the smallest, the volume fraction of rolling textures (Brass {011}<211>, S {123}<634> and Copper {112}<111>) in the center was the largest, and the volume fraction of shear textures

Foundation item: Project (2011DFR50950) supported by the International Science and Technology Cooperation Program of China; Project (51971183) supported by the National Natural Science Foundation of China; Project (cstc2019jcyj-msxmX0594) supported by the Natural Science Foundation of Chongqing, China

Corresponding author: Xian-quan JIANG; Tel: +86-13527578188; E-mail: jsq89@swu.edu.cn

DOI: 10.1016/S1003-6326(20)65338-9

(r-Cube $\{001\}\langle 110 \rangle$ and $\{112\}\langle 110 \rangle$) in $T/4$ layer (referring to the middle layer between the surface and the center) was the largest. FENG et al [10] investigated the microstructure and mechanical properties of 40 mm thick 7056 aluminum alloy in different thickness layers, and observed that the second phase was small and diffusive in the surface, large and concentrated in the center, and that in $T/4$ layer was between the two. From the surface to the center, shear textures (r-Cube $\{001\}\langle 110 \rangle$) decreased, rolling textures (Brass $\{110\}\langle 211 \rangle$, S $\{123\}\langle 634 \rangle$ and Copper $\{112\}\langle 111 \rangle$) increased, and recrystallization textures (Cube $\{001\}\langle 110 \rangle$) had little difference. ZHANG et al [11] studied the texture distribution and tensile property of 7050 aluminum alloy plate with a thickness of 120 mm, and concluded that along the thickness direction, the average sizes of the second phase and recrystallization grain gradually increased, shear textures (r-Cube $\{001\}\langle 110 \rangle$ and $\{111\}\langle 110 \rangle$) decreased, recrystallization textures (Cube $\{001\}\langle 100 \rangle$) and rolling textures (Brass $\{011\}\langle 211 \rangle$, S $\{123\}\langle 634 \rangle$ and Copper $\{112\}\langle 111 \rangle$) first decreased and then increased, and $T/4$ layer seemed to be a transition layer. There is a common law in their research results, that is, the strength of the plate presents a “V” shape or an inverted “N” shape change along the thickness direction, and the lowest value is obtained in $T/4$ layer. Earlier, similar results were also found by JONG [12]. However, up to now, there has not been relevant literature to explain the reason why the strength of $T/4$ layer is the lowest.

Large size and high homogeneity are the development direction of aluminum alloys in the

future. Regulating the size, morphology and distribution of grains is the main way to achieve the homogenization, refinement and stabilization of the structure. In this work, the relationship among rolling deformation, recovery, recrystallization and mechanical properties of 105 mm thick 5083 aluminum alloy hot rolled plate was discussed by studying the inhomogeneity of microstructure and mechanical properties along the thickness direction, in order to provide theoretical guidance for further improving the quality of aluminum alloy thick plates in industrial production.

2 Experimental

The material used in this experiment is 2500 mm × 105 mm (width × thickness) 5083 aluminum alloy hot rolled plate prepared by a domestic aluminum industry company. The chemical composition of thick plate is shown in Table 1.

Figure 1 shows the sampling diagrams of 5083 aluminum alloy thick plate. Firstly, to study the variation of microstructure and mechanical properties of thick plate along the thickness direction (normal direction, ND), sample plates were taken from one end of the plate to the center along the transverse direction (TD) and marked as A, B, C and D, respectively (Fig. 1(a)). Then, according to the sampling orientation, each sample plate was divided into ten drawing blanks along the thickness direction and numbered as Layers 1–10 from the upper surface to the lower surface (Fig. 1(b)). Finally, all the drawing blanks were

Table 1 Chemical composition of 5083 aluminum alloy thick plate (wt.%)

Si	Cu	Mg	Zn	Mn	Ti	Cr	Fe	All other elements	Al
0.163	0.004	4.434	0.026	0.678	0.012	0.104	0.238	< 0.05	Bal.

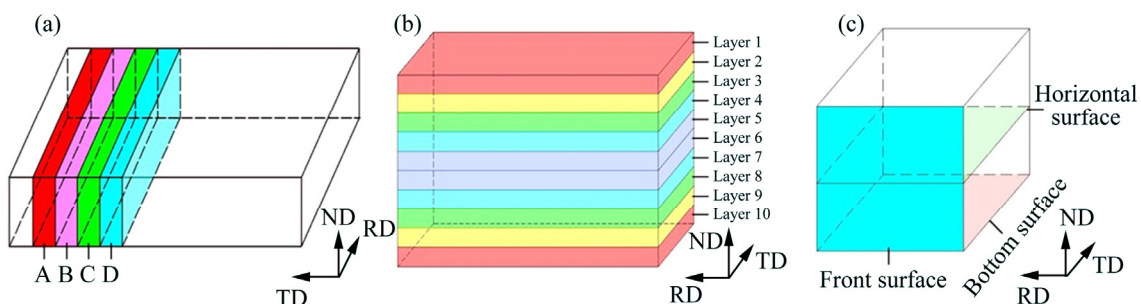


Fig. 1 Sampling diagrams of 5083 aluminum alloy thick plate: (a) Cutting method of sample plates; (b) Cutting method of drawing blanks; (c) Observation surfaces of metallographic specimens

processed into strip tensile specimens along the rolling direction (RD) meeting the GB/T 228—2002 standard.

The ultimate tensile strength (UTS), yield strength (YS) and elongation (ELO) of tensile specimens were measured at 25 °C with a tensile speed of 1 mm/min. Metallographic specimens with dimensions of 10 mm × 10 mm × 10 mm (length × width × thickness) were cut from the undeformed end of tensile specimens of Sample plate A in Layers 1–5. Considering that there was a work hardening zone on the surface of the plate, only the bottom surface, horizontal surface and front surface of metallographic specimens were mechanically ground and electrolytically polished in turn (Fig. 1(c)).

The grain structure of metallographic specimens treated by electrochemically etching in the fluoroboric acid aqueous solution to form an anodic film was observed by metallurgical microscope (OM, ZEISS AXIOVERT 200MAT). Scanning electron microscope (SEM, JEOL-6610) with electron backscatter diffraction (EBSD, OXFORD) was used to analyze the misorientation and recrystallization of grains.

3 Results and discussion

3.1 Mechanical properties

Figure 2 shows the mechanical properties of thick plate in different layers. It is obvious that the mechanical properties are inhomogeneous along the thickness direction. From the surface to the center (Layers 1–5), the UTS and YS firstly decrease, then increase and finally decrease, and the ELO presents a trend of first increasing and then decreasing. Along the width direction (Sample plates A–D), the difference of UTS, YS and ELO in the same layer is small. All test data are shown in Table 2.

To clarify the inhomogeneity of mechanical properties of the plate along the thickness direction, it is necessary to focus on the following three issues.

(1) From the surface to the center, the strength shows an inverted “N” shape change and the elongation presents a semi “U” shape change (Figs. 2(a–c)). This indicates that the strength and plasticity of the plate in Layer 5 are low.

(2) The lowest strength is not in $T/4$ layer of the plate, but shifted to Layer 2 near the surface

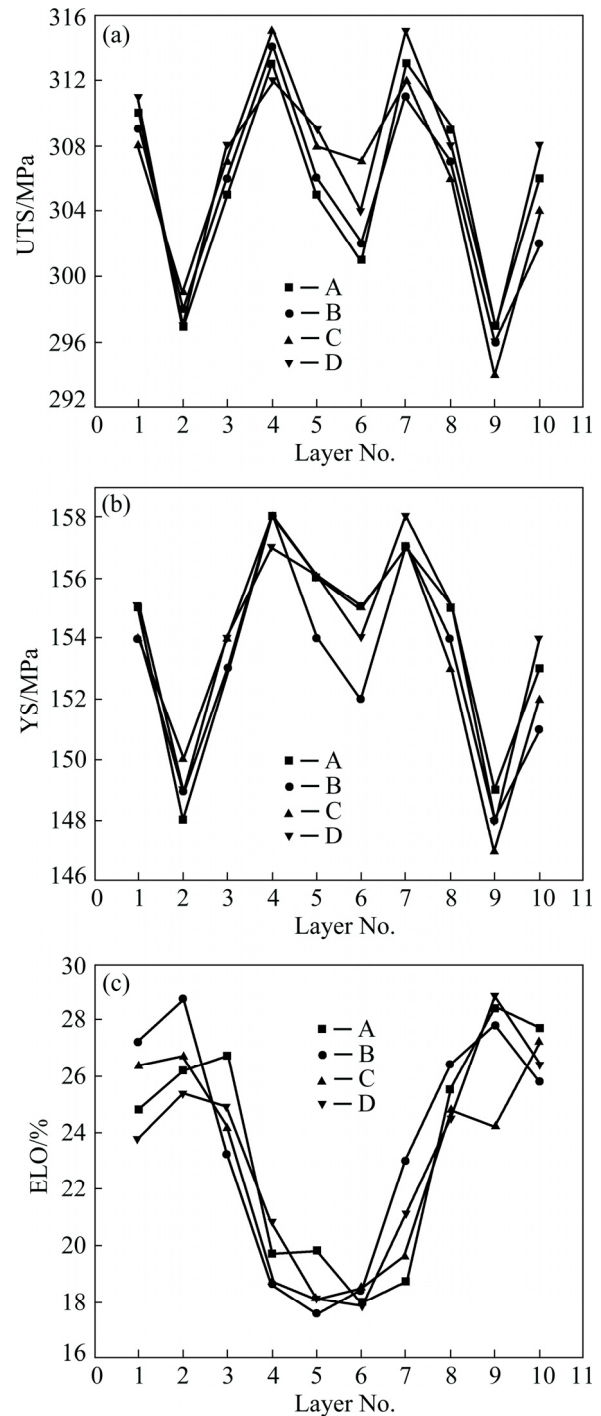


Fig. 2 Mechanical properties of thick plate in different layers: (a) UTS; (b) YS; (c) ELO

(Figs. 2(a) and (b)). This is slightly different from the previous studies, and may be related to the initial thickness of ingot, rolling deformation process, thickness of hot rolled plate and sampling method. However, the plasticity in this layer is the best (Fig. 2(c)).

(3) Layer 4 and Layer 5 are adjacent to each other, both near the central region of the plate.

Nevertheless, there is an unnegligible difference in strength (Figs. 2(a) and (b)). Taking Sample plate A as an example, the UTS and YS of Layer 4 are 2.62% and 2.60% higher than those of Layer 5, respectively (Table 2).

3.2 Microstructure

Figure 3 shows the fracture morphologies of tensile specimens. The fracture surfaces of tensile specimens are comparatively flat on the whole. Cleavage fracture areas and dimple areas are intermingled, demonstrating that the fracture mode is a mixture of ductile and brittle modes. Tearing ridges in the surface are sharp and intensive, which tend to form closed regions mostly composed of some small-dimple areas, cleavage fracture areas

and dispersed shrinkages (Fig. 3(a)). From the surface to the center, the number of tearing ridges decreases and cleavage fracture areas increase. Meanwhile, the shape of dimples gradually changes from round to parabolic and the size of shrinkages becomes larger and deeper (Figs. 3(b–d)). The central fracture primarily consists of cleavage fracture areas which enclose some sparse large-dimple areas. Grooves formed by joining shrinkages close to each other can prevent the propagation of tearing ridges and cause coarse cracks (Fig. 3(e)), which will reduce the effective area of the plate under external load [13].

According to the rolling theory [14]:

$$l/h_{cp} = 2\sqrt{R\Delta h} / (H + h) \quad (1)$$

Table 2 Mechanical properties of thick plate

Layer No.	UTS/MPa				YS/MPa				ELO/%			
	A	B	C	D	A	B	C	D	A	B	C	D
1	310	309	308	311	155	154	154	155	24.8	27.2	26.4	23.8
2	297	298	299	297	148	149	150	149	26.2	28.7	26.7	25.4
3	305	306	307	308	153	153	154	154	26.7	23.2	24.2	24.9
4	313	314	315	312	158	158	158	157	19.7	18.6	18.7	20.8
5	305	306	308	309	154	154	156	156	19.8	17.6	18.1	18.1
6	301	302	307	304	152	152	155	154	18.0	18.4	18.5	17.8
7	313	311	312	315	157	157	157	158	18.7	23.0	19.6	21.1
8	309	307	306	308	155	154	153	155	25.5	26.4	24.8	24.5
9	297	296	294	296	149	148	147	148	28.4	27.8	24.2	28.8
10	306	302	304	308	153	151	152	154	27.7	25.8	27.2	26.4

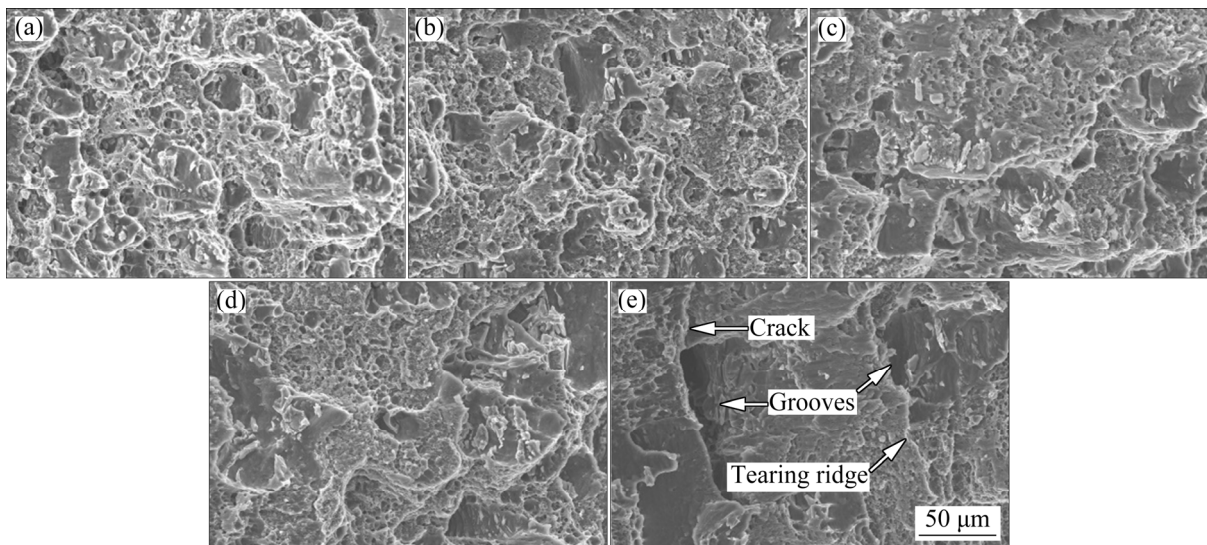


Fig. 3 Fracture morphologies of tensile specimens: (a) Layer 1; (b) Layer 2; (c) Layer 3; (d) Layer 4; (e) Layer 5

where l is the length of deformation zone, h_{cp} is the average thickness of workpiece, R is the roll radius, Δh is the increment of rolling thickness, H is the thickness of workpiece before rolling, and h is the thickness of workpiece after rolling.

When $l/h_{cp} < 1$ (referring to the earlier stage of rolling) or > 1 (referring to the later stage of rolling), additional stresses in the surface or center of the metal are different, which are manifested in the alternating change of additional compressive stress and additional tensile stress. In this experiment, the total reduction ratio of the plate is 83.3%, the reduction per pass is controlled at 10–55 mm and its value in the stable rolling process is kept at 33–38 mm. By roughly calculating, the shape coefficient of each pass deformation zone $l/h_{cp} \in [0.25, 1.35]$. It is obvious that the interior of the plate undergoes the alternation of additional stresses, certainly leading to the decline of mechanical properties [15]. Hence, it is necessary to find out the boundary region of the alternating effect. Generally, the existence of additional stresses inevitably causes additional lattice distortion which will increase the driving force of recovery and recrystallization.

The grain structures on the front (main image) and bottom (secondary image) surfaces of thick plate are shown in Fig. 4. By observing the grain morphology on the front surface of metallographic specimens, it can be seen that the plate is mainly composed of fibrous grains elongated along the

rolling direction. Deep into the center, the length of fibrous grains decreases and the width increases. Along the thickness direction in Layer 2, not only the uneven distribution of grain size is appreciably visible, but also some isolated short fibrous grains (marked with white oval frames) can be observed at certain thickness locations (Fig. 4(b)). Furthermore, starting from Layer 3, the grain boundary suddenly becomes clear (Fig. 4(c)), suggesting that the deformation degree of the plate in this layer is slighter than that in Layer 2 [16]. Considering that the strength in Layer 2 is seriously reduced, it is reasonable to suspect that this is the key position we are looking for.

A further observation of the grain morphology on the bottom surface shows that grains in Layer 4 and Layer 5 are mostly approximated to be equiaxed and some grain boundaries present serrated (marked with white arrows), implying that recrystallization occurs in these layers (Figs. 4(d) and (e)).

Figures 5 and 6 show the EBSD test results of thick plate in Layers 2, 4 and 5, separately. The black lines in Figs. 5(a), 5(c), 6(a) and 6(c) represent high angle grain boundaries ($\theta \geq 15^\circ$), and the regions with different colors represent grains with different orientations. The black lines in Figs. 5(b), 5(d), 5(g), 5(i), 6(b) and 6(d) represent low angle grain boundaries ($5^\circ < \theta < 15^\circ$, thin lines) and high angle grain boundaries (thick lines). The red region, yellow region and blue region in

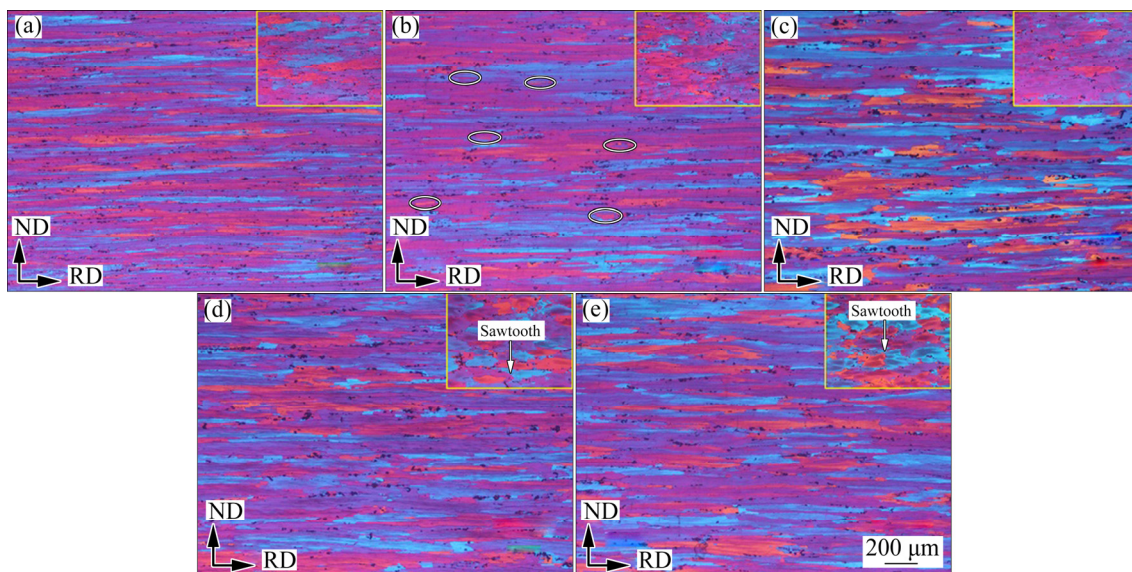


Fig. 4 Grain structures on front and bottom surfaces of thick plate: (a) Layer 1; (b) Layer 2; (c) Layer 3; (d) Layer 4; (e) Layer 5

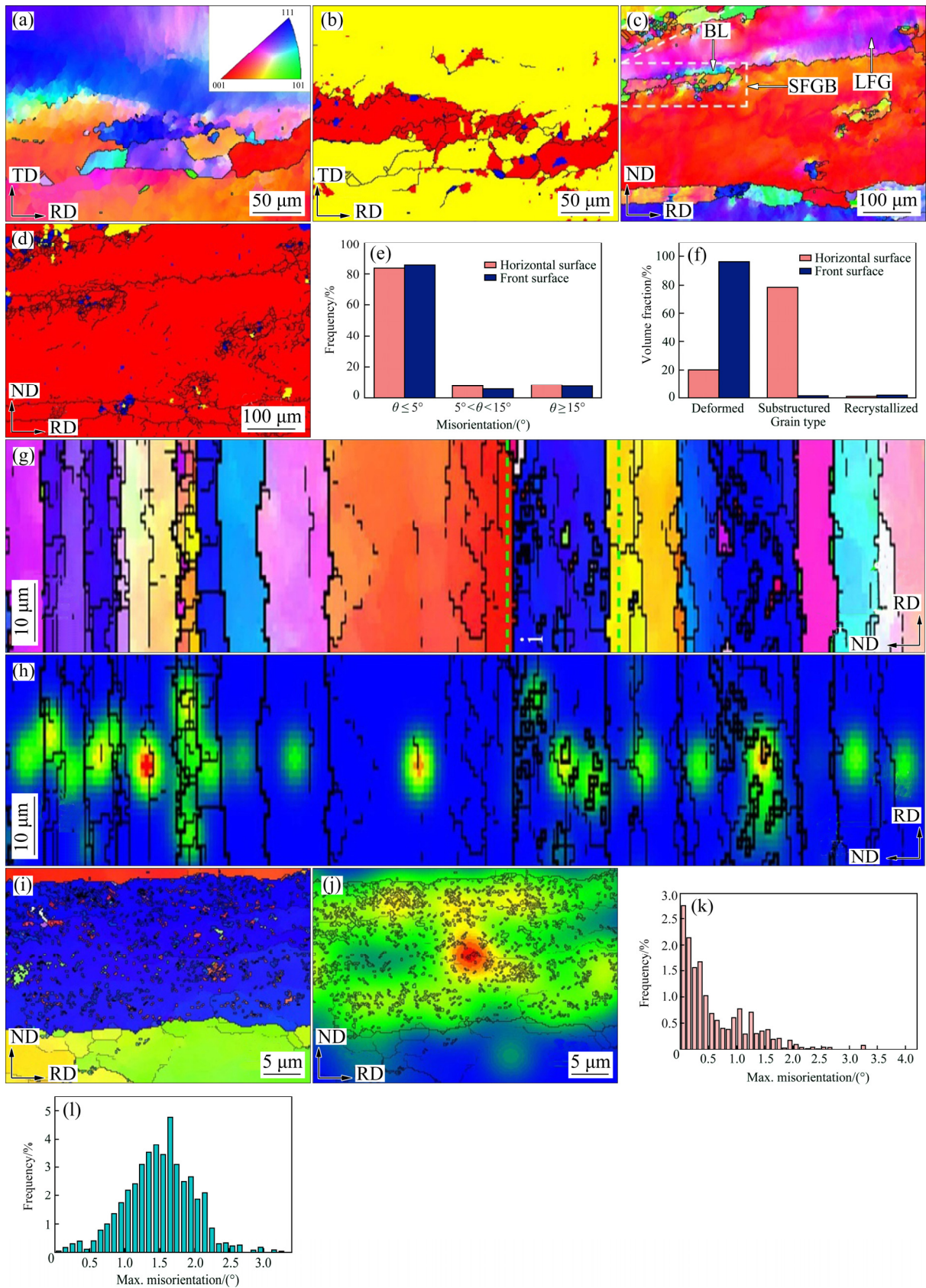


Fig. 5 EBSD test results of thick plate in Layer 2: (a–d) IPF containing misorientation angle distribution on horizontal surface selected near BL (a, b) and on front surface (c, d); (e) Frequencies of different grain boundaries; (f) Volume fractions of different grains; (g) Structural units consisting of LFG and SFG; (h) SC corresponding to (g); (i) LFG from central region of (g); (j) SC corresponding to (i); (k, l) SC histograms corresponding to (h, j), respectively

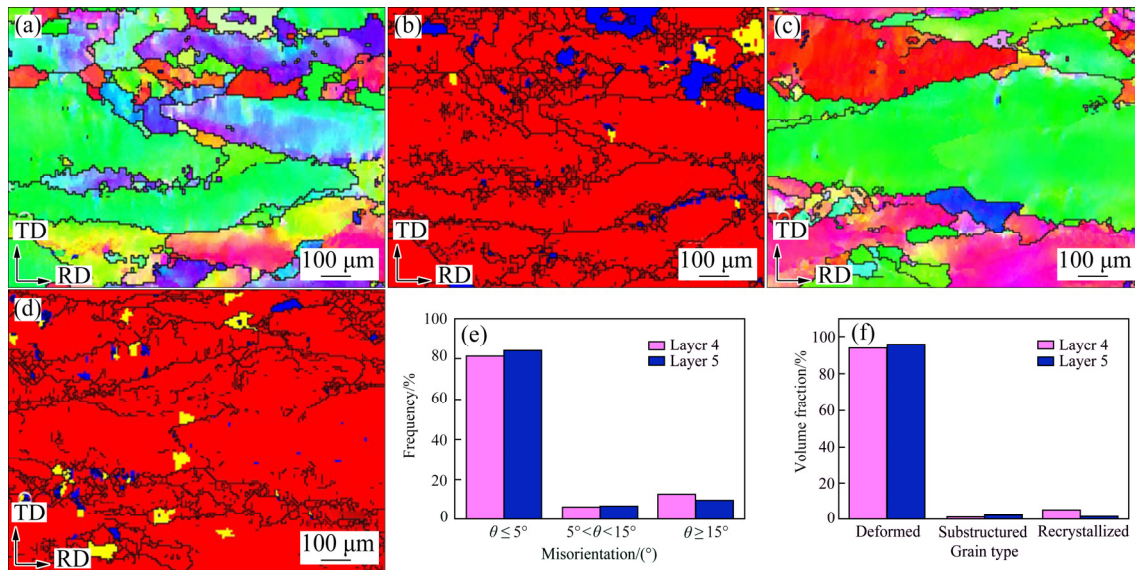


Fig. 6 EBSD test results of thick plate in Layer 4 and Layer 5: (a–d) IPF containing misorientation angle distribution on bottom surface in Layer 4 (a, b) and Layer 5 (c, d); (e) Frequencies of different grain boundaries; (f) Volume fractions of different grains

Figs. 5(b), 5(d), 6(b) and 6(d) represent the deformed grains, substructured grains and recrystallized grains respectively measured by setting a user-defined minimum angle to define a subgrain ($\theta_c=7.5^\circ$).

Figures 5(c) and (d) show the inverse pole figures containing misorientation angle distribution on the front surface in Layer 2. It can be observed that the grain growth is inhomogeneous that is manifested by a short fibrous grain band (SFGB) consisting of short fibrous grains (SFG) arranged disorderly in multiple layers between long fibrous grains (LFG). Comparing the number of black lines, it can be found that most of black lines exist near the boundary between LFG and SFGB, except for a few low angle grain boundaries distributed within the grain. Moreover, the location of high local misorientation, for example, high angle grain boundaries, is just at grain boundary of two different grains, indicating that plastic deformation is mainly concentrated on the boundary line (BL) between LFG and SFGB. Substructured grains and recrystallized grains tend to distribute in the dense area of low angle grain boundaries, which also confirms this point.

Figures 5(a) and (b) show the inverse pole figures containing misorientation angle distribution on a horizontal surface selected near the BL in Layer 2 along the thickness direction. By counting the misorientation angle distribution of grains, the

proportions of subgrain boundaries (the rotation angle of subgrain boundaries is usually $1.5^\circ-5^\circ$, therefore, $\theta \leq 5^\circ$), low angle grain boundaries and high angle grain boundaries (Table 3), and the volume fractions of deformed grains, substructured grains and recrystallized grains (Table 4) on the horizontal and front surfaces in Layer 2 can be obtained.

Table 3 Misorientation angle distribution on horizontal and front surfaces in Layer 2

Misorientation angle	Misorientation angle distribution/%	
	Horizontal surface	Front surface
$\theta \leq 5^\circ$	83.80	85.95
$5^\circ < \theta < 15^\circ$	7.71	6.22
$\theta \geq 15^\circ$	8.49	7.83

Table 4 Volume fractions of recrystallization on horizontal and front surfaces in Layer 2

Grain type	Volume fraction/%	
	Horizontal surface	Front surface
Deformed	19.99	96.53
Substructured	79.05	1.52
Recrystallized	0.96	1.95

According to the characteristics of rolling, the microstructure and mechanical properties of two adjacent points along the width direction are similar on different horizontal surfaces of the plate in the

same thickness layer (Figs. 2, 4, Table 2). Here, if a LFG and a SFGB along the thickness direction are regarded as a basic structural unit, Layer 2 consists of several similar structural units (Fig. 5(g)). It can be considered that the misorientation angle distribution of a structural unit on the front surface of the plate can represent the average state of that on all horizontal surfaces in the same thickness layer to a certain extent. The proportions of subgrain boundaries, low angle grain boundaries and high angle grain boundaries on the horizontal surface are similar to those on the front surface, which illustrates this view (Fig. 5(e), Table 3). Abnormally, the volume fraction of substructured grains on the horizontal surface is about 52 times as large as that on the front surface, and the volume fractions of deformed grains and recrystallized grains on the horizontal surface are about 20.71% and 49.23% of those on the front surface successively, indicating that there is an exceptionally strong recovery occurring on the horizontal surface during the hot rolling (Fig. 5(f), Table 4). Additionally, the plastic deformation on the horizontal surface corresponds to the grain recovery. There is no doubt that the horizontal surface mentioned above is very special for Layer 2.

Figures 5(h) and (j) show the strain contouring (SC) of thick plate in Layer 2 along the thickness direction measured by setting an appropriate half-width value of 5 μm . The detection area of Fig. 5(h) is the same as that of Fig. 5(g). It can be clearly seen that the high strain zone (warm color zone) tends to appear in the dense area of low angle grain boundaries. Influenced by the distribution of low angle grain boundaries, the high strain zone distributes alternately along the thickness direction. The peak and mean values of SC histogram occur at 0.05° and 1.55° , respectively (Fig. 5(k)). The detection area of Fig. 5(j) is the same as that of Fig. 5(i) which corresponds to the central region of Fig. 5(g). It can be observed that the strain in the grain is uneven. Generally, the deformation in the grain is more uniform and consistent than that at grain boundary. However, the high strain zone primarily exists in the grain center, and next spreads near the grain boundary. The peak and mean values of SC histogram occur at 1.65° and 0.85° , respectively (Fig. 5(l)), which have a big difference with those of Fig. 5(k), illustrating that the forming

cause of high strain zone in the grain center is different from that near the BL. In the vicinity of the BL, there will be additional stresses during the hot rolling due to different deformability of LFG and SFGB. Nevertheless, the plate in Layer 2 exhibits excellent plasticity (Fig. 2(c)), possibly benefiting from the alternating layered distribution of LFG and SFGB. This distribution is conducive to dispersing the plastic deformation concentrated on the BL in time to reduce crack initiation and delay its propagation [17,18].

Figures 6(a–d) show the inverse pole figures containing misorientation angle distribution on the bottom surface in Layer 4 and Layer 5, separately. It can be seen that the bottom surface is composed of many grains with different sizes, whose arrangement is confused. The grain coarsening in Layer 5 is more serious due to its proximity to the center (Figs. 6(a) and (c)). Similarly, low angle grain boundaries and high local misorientation are inclined to distribute between grains, suggesting that plastic deformation primarily occurs at grain boundary (Figs. 6(b) and (d)). Moreover, recrystallized grains are easy to nucleate near the substructured grains, indicating that recovery has a priority in the center of the plate during the hot rolling. By counting the misorientation angle distribution of grains, the proportions of subgrain boundaries, low angle grain boundaries and high angle grain boundaries (Table 5), and volume fractions of deformed grains, substructured grains and recrystallized grains (Table 6) on the bottom surface in Layer 4 and Layer 5 can be obtained. The proportions of subgrain boundaries and low angle grain boundaries in Layer 4 are lower than those in Layer 5, suggesting that the degree of recovery or recrystallization of the plate is greater (Fig. 6(e), Table 5). The volume fraction of substructured grains in Layer 4 is about 54.63% of that in Layer 5, and the volume fraction of recrystallized grains in Layer 4 is about 3.33 times as large as that in Layer 5 (Fig. 6(f), Table 6). This result is in a good agreement with the rolling characteristics of aluminum alloy thick plates. That is, deformation is gradually penetrated into the center of the plate, meaning that Layer 5 with higher temperature, smaller deformation degree and more lagging critical deformation of recrystallization is prone to recover rather than recrystallize, while Layer 4 tends to recrystallize.

Table 5 Misorientation angle distribution on bottom surface in Layer 4 and Layer 5

Misorientation angle	Misorientation angle distribution/%	
	Layer 4	Layer 5
$\theta \leq 5^\circ$	81.41	84.12
$5^\circ < \theta < 15^\circ$	6.06	6.52
$\theta \geq 15^\circ$	12.53	9.36

Table 6 Volume fractions of recrystallization on bottom surface in Layer 4 and Layer 5

Grain type	Volume fraction/%	
	Layer 4	Layer 5
Deformed	93.86	96.35
Substructured	1.18	2.16
Recrystallized	4.96	1.49

4 Conclusions

(1) The mechanical properties of 5083 aluminum alloy thick plate are inhomogeneous along the thickness direction. From the surface to the center, the strength shows an inverted “N” shape change and the elongation presents a semi “U” shape change.

(2) The reason for the shifting of the lowest strength to Layer 2 may be that the main deformation zone of the plate is located near the surface in a long period by calculating the shape coefficient of each pass deformation zone l/h_{cp} .

(3) Layer 2 consists of several similar structural units composed of LFG and SFGB. This alternating layered distribution is conducive to improving the plasticity by dispersing the plastic deformation concentrated on the BL.

(4) During the hot rolling, the alternation of additional stresses induced by the different deformability of LFG and SFG in Layer 2 will eventually cause a decrease in strength.

(5) The closer the location to the center of the plate is, the more likely the recovery rather than the recrystallization occurs. This is the possible reason for the unnegligible difference in strength between Layer 4 and Layer 5. Furthermore, the low strength and elongation in Layer 5 are related to the original casting defects.

References

[1] LEE S W, YEH J W. Superplasticity of 5083 alloys with Zr

and Mn additions produced by reciprocating extrusion [J]. *Materials Science and Engineering A*, 2007, 460–461: 409–419.

- [2] CHE Hong-mei, JIANG Xian-quan, QIAO Nan, LIU Xiao-kui. Effects of Er/Sr/Cu additions on the microstructure and mechanical properties of Al–Mg alloy during hot extrusion [J]. *Journal of Alloys and Compounds*, 2017, 708: 662–670.
- [3] ZHANG Cun-sheng, WANG Cui-xue, GUO Ran, ZHAO Guo-qun, CHEN Liang, SUN Wen-chao, WANG Xie-bin. Investigation of dynamic recrystallization and modeling of microstructure evolution of an Al–Mg–Si aluminum alloy during high-temperature deformation [J]. *Journal of Alloys and Compounds*, 2019, 773: 59–70.
- [4] SINGH D, RAO P N, JAYAGANTHAN R. Effect of deformation temperature on mechanical properties of ultrafine grained Al–Mg alloys processed by rolling [J]. *Materials and Design*, 2013, 50: 646–655.
- [5] XIA S L, MA M, ZHANG J X, WANG W X, LIU W C. Effect of heating rate on the microstructure, texture and tensile properties of continuous cast AA5083 aluminum alloy [J]. *Materials Science and Engineering A*, 2014, 609: 168–176.
- [6] CHEN Xiang, HUANG Guang-sheng, LIU Shuai-shuai, HAN Ting-zhuang, JIANG Bin, TANG Ai-tao, ZHU Yun-tian, PAN Fu-sheng. Grain refinement and mechanical properties of pure aluminum processed by accumulative extrusion bonding [J]. *Transactions of Nonferrous Metals Society of China*, 2019, 29: 437–447.
- [7] MEI L, CHEN X P, HUANG G J, LIU Q. Improvement of mechanical properties of a cryorolled Al–Mg–Si alloy through warm rolling and aging [J]. *Journal of Alloys and Compounds*, 2019, 777: 259–263.
- [8] ZHAO Kuo, LIU Jian-hua, YU Mei, LI Song-mei. Through-thickness inhomogeneity of precipitate distribution and pitting corrosion behavior of Al–Li alloy thick plate [J]. *Transactions of Nonferrous Metals Society of China*, 2019, 29: 1793–1802.
- [9] CHANG Jiang-yu, CHEN Song-yi, CHEN Kang-hua, ZHOU Liang, YUAN Ding-ling. Numerical simulation and experimental investigation of rolling deformation inhomogeneity of 7056 aluminum alloy thick plate [J]. *Journal of Central South University: Science and Technology*, 2018, 49: 1914–1921. (in Chinese)
- [10] FENG Shuai, SUN Li-ming, CHEN Zhi-guo, ZHENG Zi-qiao, LI Jin-feng. Microstructure and mechanical properties of 7056 aluminum alloy thick plates [J]. *Rare Metal Materials and Engineering*, 2018, 47: 3088–3095. (in Chinese)
- [11] ZHANG Xin-ming, HAN Nian-mei, LIU Sheng-dan, SONG Feng-xuan, ZENG Rui-lin, HUANG Le-yu. Inhomogeneity of texture, tensile property and fracture toughness of 7050 aluminum alloy thick plate [J]. *The Chinese Journal of Nonferrous Metals*, 2010, 20: 202–208. (in Chinese)
- [12] de JONG H F. Thickness direction inhomogeneity of mechanical properties and fracture toughness as observed in aluminium 7075-T651 plate material [J]. *Engineering*

Fracture Mechanics, 1980, 13: 175–192.

- [13] RAN Guang, ZHOU Jing-en, WANG Yong-fang. Study on tensile properties and fractography of cast A356 aluminum alloy [J]. Rare Metal Materials and Engineering, 2006, 35: 1620–1624. (in Chinese)
- [14] ZHONG Li, MA Ying-yi, XIE Yan-cui. Production technology of aluminum alloy plates [M]. Beijing: Metallurgical Industry Press, 2009. (in Chinese)
- [15] XU Wei-feng, LIU Jin-he, CHEN Dao-lun. Study on nonhomogeneity of low-cycle fatigue properties along thickness direction of plate for friction stir welded aluminum alloy joint [J]. Acta Metallurgica Sinica, 2015, 51: 587–596. (in Chinese)
- [16] ZENG Qiang, WEN Xi-yu, ZHAI Tong-guang. Texture evolution rate in continuous cast AA5052 aluminum alloy during single pass hot rolling [J]. Materials Science and Engineering A, 2008, 476: 290–300.
- [17] BLOYER D R, RAO K T V, RITCHIE R O. Fracture toughness and r-curve behavior of laminated brittle-matrix composites [J]. Metallurgical and Materials Transactions A, 1998, 29: 2483–2496.
- [18] WU Hao, FAN Guo-hua, HUANG Meng, GENG Lin, CUI Xi-ping, XIE Hong-lan. Deformation behavior of brittle/ductile multilayered composites under interface constraint effect [J]. International Journal of Plasticity, 2017, 89: 96–109.

5083 铝合金厚板显微组织与力学性能的关系

余欣未^{1,2}, 蒋显全^{1,2}, 王浦全¹, 唐彬彬¹, 陈康¹, 刘玉洁¹, 曹伟男¹

1. 西南大学 材料与能源学院, 重庆 400715;

2. 重庆市科学技术研究院 新材料研究中心, 重庆 401123

摘要: 采用金相显微镜、扫描电镜和拉伸试验机研究厚度为 105 mm 5083 铝合金热轧板的显微组织与力学性能, 解释厚板力学性能不均匀性中存在的三大特征问题。结果表明: 轧板厚度方向力学性能具有不均匀性, 从表面到中心强度呈倒“N”形变化, 伸长率呈半“U”形变化。在靠近表面的一个特殊层(第 2 层)上发现若干个由长纤维状晶粒(LFG)和短纤维状晶粒带(SFGB)构成的相似结构单元, 这种长纤维状晶粒和短纤维状晶粒带的交替层状分布有利于通过分散集中在两者之间晶界线(BL)上的塑性变形来提高塑性。但是, 在热轧过程中两种不同变形能力的晶粒会引起附加应力的交替分布, 致使强度降低。越靠近轧板中心, 越容易发生回复而非再结晶, 这可能是近中心区域(第 4 层和第 5 层)强度存在一个不可忽视的差值的原因。

关键词: 铝合金厚板; 力学性能; 不均匀性; 纤维状晶粒; 动态回复; 动态再结晶

(Edited by Wei-ping CHEN)